UNIQUE DEFICITS IN PLACE CODING ACROSS SUBFIELDS OF THE HIPPOCAMPUS IN A MOUSE MODEL OF TEMPORAL LOBE EPILEPSY.

Brittney L. Boublil[1], Cathy B. Dang[1], Gergely Tarcsay[1], Laura A. Ewell[1,2,3]

[1]Anatomy and Neurobiology, School of Medicine, University of California, Irvine, Irvine, CA, USA
[2]Neurobiology of Brain and Behavior, Charlie Dunlop School of Biological Sciences, University of California, Irvine, Irvine, CA, USA
[3]Center for Learning and Memory, University of California, Irvine, Irvine, CA, USA

ABSTRACT

Memory problems are comorbid with Temporal Lobe Epilepsy (TLE). Animal models of TLE reveal impairments in spatial firing fields of hippocampal place cells, providing a potential neural substrate for memory problems. Each subfield of the hippocampus carries out unique aspects of spatial memory, yet little is known about how individual subfields are perturbed. Here, we investigated the spatial coding properties of the three major subfields of the hippocampus. Single unit recordings were made from CA1, CA3 and the dentate gyrus (DG) of mice induced with epilepsy (N = 10, 6M/4F) using the supra-hippocampal kainate model and in control mice injected with saline (N = 6, 3M/3F). Place cell activity was measured while mice foraged in highly familiar environments to assess basic place cell properties and in novel environments to assess remapping. A lower percentage of cells were classified as place cells in CA1 of epileptic mice, whereas percentages were similar in CA3 and DG compared to control. Place fields of CA1 and CA3 cells were less coherent, while DG fields were less stable. All regions constructed new distinct maps within the first session of exposure to a novel environment, however new maps in CA3 were not stable. These results point to specific deficits within subfields of the hippocampus, which may indicate that there are different cellular and network mechanisms at play. Such heterogeneity would be predicted to contribute differently to memory deficits and suggests that interventions for treatment may need to be tailored.

INTRODUCTION

Memory comorbidity is common in epilepsy and greatly impacts patient's quality of life (1, 2). Disease associated injury to temporal lobe structures is commonly thought to be the culprit. Recent work, however, highlights the role of altered network function during interictal periods (3), which is significant because network function is a rescuable target. In the case of temporal lobe epilepsy (TLE), it is well established that behaviorally relevant firing patterns of hippocampal place cells (neurons with spatially tuned firing patterns) are disrupted in multiple rodent models (4, 5, 6, 7, 8, 9). Disrupted spatial coding of hippocampal place cells is a strong candidate for the neural substrate of impaired memory in TLE.

The hippocampus comprises several subfields – with each providing distinct roles in spatial memory (10, 11). Signals enter the hippocampus at the dentate gyrus (DG) and

then pass on to area CA3 and finally to area CA1, the output structure. The overwhelming majority of studies of place coding in epilepsy have focused on area CA1 despite circuit and functional characteristics of the DG and area CA3 that make them potentially more vulnerable in TLE. The DG is typically a sparsely activated structure thought to perform pattern separation (12, 13), the transformation of cortical signals into maximally distinct representations to store in CA3. In TLE, the DG undergoes massive rewiring and experiences significant inhibitory interneuron loss (14, 15, 16, 17, 18, 19). Area CA3, which sits at the core of hippocampal processing, has unique anatomy compared to the other hippocampal subfields – it is a highly recurrent structure (i.e., auto-associative) in which neurons receive input from their own axons, and commissural connections from the contralateral CA3. It is proposed that such recurrence supports the storage and recall of ensemble representations of distinct features of environments (separated by the DG) (20) and supports temporal ordering of experience (21). Classically, recurrence in CA3 is also thought to underly the susceptibility of the hippocampus to hypersynchronous neural activity observed during seizures and interictal discharges.

We performed single unit recordings in freely moving mice, targeting the three major subfields of the hippocampus. Employing the supra-hippocampal kainic acid model of chronic TLE, we tested how TLE impacts place coding across subfields. We recorded while mice foraged in highly familiar environments and during exploration of a novel environment. Familiar environment recordings provided a baseline understanding of region-specific place codes, while novel room recordings allowed us to assess pattern separation mechanisms and storage/stability of new maps.

MATERIALS AND METHODS

Subjects

A total of 16 C57BL/6 mice (nine males and seven females) were used for this study. Mice were individually housed on a reversed 12/12-hour light/dark cycle. The weights of all mice were maintained on an *ad libitum* diet except during the open field foraging task, when mice were food restricted to maintain 85% of their baseline weight. All experimental procedures were approved by the Institutional Animal Care and Use Committee (IACUC) at the University of California, Irvine.

Induction procedure for supra-hippocampal kainate model

All surgeries were performed using aseptic procedures. Mice (12 weeks old) were initially anesthetized with isoflurane gas and transferred to a Kopf stereotaxic instrument, where they were positioned and secured with an anesthesia mask and non-rupture ear bars. Anesthesia was maintained throughout the surgery at 1-2% isoflurane delivered in O_2 at 1 L/min and body temperature was maintained at 37–38°C using reusable gel heat packs. Eyes were protected with a lubricating eye ointment. Carprofen (Patterson Veterinary, 5 mg/kg) was administered subcutaneously as an analgesic. The scalp was prepared by removing the hair and washing the scalp with iodine. Lidocaine (Patterson Veterinary, 4 mg/kg) was injected subcutaneously under the scalp, and a midline incision was made.

The skin was retracted, and a craniotomy was made above the hippocampus (AP: -2.0 mm, ML: +1.5 mm from bregma) using a carbide bur.

Kainic acid (KA) (Tocris) was dissolved in saline to provide a solution with a concentration of 20 mM (22, 23, 24, 25). A glass pipette was lowered into the brain (DV: -0.8 mm from dura) and left in place for a minimum of 1 minute before the injection. 70 nL of KA (or sterile saline for controls) was injected using a custom microinjection system (Narishige International, #MO-10), over the span of 2 min. The glass pipette remained in place for an additional 1 minute following the injection to prevent the backflow of the solution up the needle tract. The incision was closed with absorbable sutures. *Status epilepticus* was terminated 4 hours later with a subcutaneous injection of either lorazepam (West-Ward, 7.5 mg/kg) or diazepam (Patterson Veterinary, 20 mg/kg). Lorazepam/Diazepam was not injected for saline control mice.

Implantation of Open Ephys ShuttleDrive

Four weeks after *status epilepticus*, mice were implanted with an Open Ephys ShuttleDrive (26), which is composed of 16 individually moving tetrodes. Surgical preparation was the same as described above. Once anesthetized and secured to the stereotaxic instrument, buprenorphine (Patterson Veterinary, 0.1 mg/kg) was administered subcutaneously as an analgesic. Once the skull was exposed, additional surface area was created to improve the bonding of the dental composite by scoring the skull bone and by making shallow divots on the skull's surface using a carbide bur. Optibond was applied over the prepared skull and cured with UV light. Dexamethasone (Patterson Veterinary, 4 mg/kg) was injected intraperitoneally to reduce swelling in the brain. A craniotomy was made over the cerebellum behind lambda for the ground electrode, which was secured to the skull using an optical dental composite. A second, larger craniotomy was made above the hippocampus (AP: -2.0 mm, ML: +1.5 mm from bregma) using a trephine stainless steel bur. Surgilube was applied to the surface of the brain, and the bundle of the drive was dipped in mineral oil. The drive was lowered until the bundle rested on the surface of the brain and secured to the skull using optical dental composite and UV light. The ground of the drive and the implanted ground wire were soldered together, and the excess ground wire was trimmed and encased in the dental composite to protect the ground wire and blunt any sharp edges. Mice were removed from the stereotaxic frame and carprofen was administered subcutaneously as an analgesic. Immediately after the surgery, each tetrode was turned down 450 μm into cortex.

Data acquisition during random foraging in an open field

Single units and video were recorded simultaneously during all rest and behavioral sessions. The electrophysiological data were synchronized with video using Bonsai (27, 28) and data were acquired using the Open Ephys Acquisition Board (28). Following a one-week postoperative recovery period, mice were food restricted to maintain 85% of their baseline weight. Mice were trained to randomly forage for food reward (Bio-Serv, Bacon Flavored Foraging Crumbles, #F5783) in an open, black, square arena (diameter

= 41 cm, height = 36 cm), with a checkered cue card. Behavioral sessions included: a 20-minute rest session before the first foraging session, four 10-minute foraging sessions with 5 minutes of rest in between, and a 20-minute rest session after the last foraging session. During this training period, tetrodes were strategically advanced into the hippocampus, targeting subfields CA1, CA3, and DG.

Once mice covered the arena consistently during behavioral sessions and tetrodes were in their target location, mice were then exposed to a novel arena. The novel arena was an open, white circle arena (diameter = 49 cm, height = 33 cm), with a checkered cue card. The foraging session sequence began with one session in the familiar square arena, followed by four sessions in the novel, circle arena, and ended with the last session in the familiar arena (Figure 3A). Again, foraging sessions were flanked by 20-minute rest sessions.

Histology and DG dispersion scoring protocol

At the conclusion of the experiment, mice received an overdose of sodium pentobarbital. Mice were perfused intracardially with 0.37% sulfide solution, followed by 4% paraformaldehyde (PFA) in phosphate-buffered saline (PBS). Brains were extracted and stored in the PFA solution overnight and then transferred to 30% sucrose in PBS. Brains were sectioned using a freezing microtome. 50 µm coronal sections were collected through the hippocampal segment with electrode tracks. Each section was mounted onto microscope slides using a gelatin solution in PBS. Mounted sections were double stained with TIMM sulfide silver and cresyl violet to visualize tetrode tracks. The final position of each tetrode was reconstructed using serial sections. Data from tetrodes were only included in the data analysis if the tetrode's final position was determined to be in CA1, CA3, or DG cell layers.

DG dispersion measurements were determined by an investigator that manually measured the thickness of the upper blade of the DG for three consecutive sections of dorsal hippocampus, ipsilateral to the injection, for saline control and KA mice (Figure S1). The thickness for the three sections was averaged to obtain a measure of DG dispersion for each mouse.

Interictal spike (IS) detection on local field potential (LFP)

All signal processing was done in MATLAB (MathWorks, R2022b). The IS detection procedure used was based on Yi et al. (2025) (29). An LFP channel was selected from a hippocampal tetrode for each KA mouse, during a familiar rest and a behavioral session. The LFP was down-sampled to 1 kHz and band-pass filtered (Table 1). Spikes that had peaks with a minimum peak prominence and peak height above a tuned threshold were counted as IS.

Data processing and place cell classification

Electrophysiological data from each rest and behavioral session were high-pass filtered, and background subtracted for clustering into putative single units using Kilosort (30). Putative single units were then manually curated in Phy (https://github.com/cortex-lab/phy), where any cluster that did not show stable waveform amplitudes or clear refractory periods were discarded. The position of mice was estimated using DeepLabCut (31, 32) and correlated with synchronized spike times. Using position, instantaneous running speeds for each session were calculated. Position data and their respective spike times from periods of immobility, defined as a running speed less than 2 cm/s, were excluded.

Putative principal neurons were distinguished from putative interneurons using a 10 Hz average firing rate criterion. Principal neurons were then categorized as either active or inactive using a peak firing rate criterion of 2 Hz. Inactive neurons (peak firing rate < 2 Hz) were excluded from the analysis. Active, putative principal neurons then underwent a shuffling procedure to classify them as either place or non-place cells. First, spatial information for each behavioral session was calculated using the following equation (33, 34):

$$Information = \sum_{i=1}^{N} p_i \frac{\lambda_i}{\bar{\lambda}} \log_2 \frac{\lambda_i}{\bar{\lambda}},\ p_i = \frac{t_i}{\sum_{i=1}^{N} t_i},\ \bar{\lambda} = \sum_{i=1}^{N} p_i \lambda_i$$

where i represents the 2 cm bins of the environment, p_i is the occupancy probability and λ_i is the mean firing rate of a given bin i, and λ is the overall mean firing rate of a cell. The session with the highest spatial information for a given cell was selected and then underwent a circular shuffling procedure (1000 shuffles in which spatial positions were time-shifted by a random amount and spatial information was recalculated). Putative principal neurons were classified as place cells if the if the original distribution was greater than the 95th percentile of the shuffled distribution.

Spatial analysis

Rate maps. Rate maps of neuronal firing for each behavioral session were constructed as described in Skaggs et al. (1996) (34). Environments were divided into 2 cm bins, and the firing rate at each location was calculated by expanding a circle centered on a given bin until it met the following criterion:

$$N_{spikes} > \frac{\alpha}{N_{occ}^2 r^2}$$

where N_{spikes} is the number of spikes, N_{occ} is the number of occupancy samples with a sampling frequency of 30 Hz, r is the radius of the circle in bins, and α is a scaling factor set as 10,000. The firing rate at each location was calculated as the following:

$$Sampling\ frequency \times \left(\frac{N_{spikes}}{N_{occ}}\right)$$

Spatial correlations. To assess spatial stability within a session, rate maps were split into the first and second half of the session. The correlation coefficients (r) between half maps were calculated using Pearson's correlation. To assess spatial stability across sessions, correlation coefficients were calculated between two behavioral sessions using Pearson's correlation.

Spatial coherence. Spatial autocorrelation of the rate map was calculated as a measure of how neighboring pixels are related to each other (35).

Sparsity. Calculated using the following equation (33, 34):

$$Sparsity = \frac{\lambda^2}{\sum_i^N p_i(\lambda_i)^2}$$

Spatial selectivity. Peak firing rate (in the spatial bin with the highest rate) divided by the average firing rate calculated across all spatial bins.

Statistical analysis

Statistics were performed using MATLAB (MathWorks, R2022b) software. Statistical significance was determined using one of the following tests: Chi-squared test, Wilcoxon rank sum test, Two-sample Kolmogorov-Smirnov test, Two-sample F-test for equal variances, One-way ANOVA, or Wilcoxon signed rank test. Significant statistical differences were indicated with $*p \leq 0.05$, $**p \leq 0.01$, $***p \leq 0.001$, or $****p \leq 0.0001$.

RESULTS

Proportion of place cells are reduced in hippocampal subfield CA1 in KA mice

Our study sought to explore the impact of chronic, focal TLE on hippocampal function. Here, we investigated spatial coding properties of the three hippocampal subfields (CA1, CA3, and DG) in epileptic mice, ipsilateral to the epileptic focus. We employed the supra-hippocampal kainate model of TLE (22, 36, 37). Mice were injected into the cortex above hippocampus with kainic acid (KA; N = 10, 6 male/4 female) or saline as a control (N = 6, 3 male/3 female). Four weeks post-injection, mice were implanted with an Open Ephys ShuttleDrive (26) and electrophysiological data from the three hippocampal subfields were obtained while mice foraged in a familiar environment (Figure 1A-B). Consistent with previous reports of this epilepsy model, we observed interictal spikes (IS) in all KA mice, with relatively low rates during foraging (average IS rate = 0.11 spikes/s) (Table 1).

We obtained recordings from principal neurons from each hippocampal subfield while mice foraged in familiar spatial environments. There was no significant difference in the distribution of peak firing rates between control and KA mice in any subregion (Figure 1C and Table 2, CA1: z = 0.40, p = 0.69; CA3: z = 1.89, p = 0.06; DG: z = 0.86, p = 0.39, Wilcoxon rank sum test). Next, we considered place-firing properties of neurons that were active during behavior (> 2 Hz peak firing rate). Place cells were classified as cells with

significant spatial information (Figure 1D, *see methods*). We found that the proportion of place cells was significantly lower in CA1 of KA mice compared to control mice (Figure 1E, $\chi^2(1,163) = 12.01$, $p \leq 0.001$, Chi-squared test). In contrast, there was no significant difference in the proportion of place cells between control and KA mice for CA3 (Figure 1E, $\chi^2(1,133) = 0.20$, $p = 0.66$, Chi-squared test) or DG (Figure 1E, $\chi^2(1,61) = 0.13$, $p = 0.72$, Chi-squared test). Taken together, despite similar activity levels in KA and control mice, we observe general place coding deficits in CA1.

Properties of spatial coding in familiar environments are impaired in KA mice

Next, we assessed the quality of place coding in familiar environments (Figure 2 and Table 3). We observed a significant reduction in the stability of place cells in DG of KA mice compared to control mice (Figure 2B, D = 0.63, $p \leq 0.05$, Two-sample Kolmogorov-Smirnov test). There was no significant difference in the stability of place cells between control and KA mice for CA1 (Figure 2B, D = 0.18, $p = 0.35$, Two-sample Kolmogorov-Smirnov test) and CA3 (Figure 2B, D = 0.21, $p = 0.30$, Two-sample Kolmogorov-Smirnov test). Despite exhibiting stability, the spatial coherence of CA1 and CA3 place maps from KA mice were reduced (Figure 2C, CA1: z = 3.95, $p \leq 0.0001$; CA3: z = 2.54, $p \leq 0.01$, Wilcoxon rank sum test), while spatial coherence was maintained in DG (Figure 2C, DG: z = 1.36, $p = 0.17$, Wilcoxon rank sum test). We did not observe any significant changes in other spatial properties of place cells (Table 3). Additionally, we found that there was increased variance in spatial correlation and coherence of CA3 place maps of KA mice, but these changes could not be explained by the specific subareas of CA3 (Figure S1) or the severity of histopathology (Figure S1). Together, these data point towards subregion-specific impairments in place coding across the hippocampal circuit in KA mice.

Spatial stability of newly formed maps in a novel environment are impaired in KA mice

We next examined another feature of hippocampal place cells, the ability to quickly establish new representations (i.e., place maps) upon entering a completely novel environment (Figure 3). Electrophysiological recordings were obtained from the three hippocampal subfields (CA1, CA3, and DG) while mice explored both a familiar and a novel environment (Figure 3A-B). We observed that all subfields of the hippocampus remapped between familiar and novel environments (i.e., formed unique spatial representations) for control mice (Figure 3C, black, CA1: z = 5.47, $p \leq 0.0001$; CA3: z = 3.72, $p \leq 0.001$; DG: z = n/a, $p \leq 0.001$, Wilcoxon signed rank test) and KA mice (Figure 3C, pink,CA1: z = 3.66, $p \leq 0.001$; CA3: z = 4.62, $p \leq 0.0001$; DG: z = 4.33, $p \leq 0.0001$, Wilcoxon signed rank test). Additionally, the extent of remapping was of similar magnitude between control and KA mice for all subregions (Figure 3D, CA1: z = -0.90, $p = 0.37$; CA3: z = -0.80, $p = 0.42$; DG: z = 0.45, $p = 0.75$, Wilcoxon signed rank test). Next, we assessed the stability of the newly formed maps across multiple exposures to the same novel environment (Figure 3E). We observed a significant decrease in the stability of newly formed maps in CA3 of KA mice (Figure 3E, z = 2.46, $p \leq 0.01$, Wilcoxon rank sum test). Finally, there was no significant difference in the stability of the newly formed place maps between control and KA mice for CA1 (Figure 3E, z = -1.39, $p = 0.16$, Wilcoxon rank sum test) or DG (Figure 3E, z = 0, $p = 1$, Wilcoxon rank sum test). While these findings

demonstrate that remapping is intact in KA mice across the major hippocampal subregions, we find a reduction in the stability of place fields in CA3 of KA mice.

DISCUSSION

We show unique alterations in place representations of hippocampal subfields in a rodent model of focal temporal lobe epilepsy (TLE). In familiar environments, there were fewer place cells in CA1 of epileptic mice and those remaining exhibited a reduction in spatial coherence. Our findings are consistent with results from previous studies of CA1 place coding in TLE (4, 5, 6, 7, 8, 9). In addition, we observed a reduction in the stability of DG place cells, and a reduction in spatial coherence of CA3 place cells. Loss of inhibition within the hippocampal circuit is widely reported in TLE, and others have shown that disrupted inhibition in DG/CA3 impacts place coding in CA1 (38, 39, 40). Another potential contributor to the disparate deficits we observe is the upstream input coming from the entorhinal cortex, which differentially innervates the DG/CA3 and CA1 subfields via the perforant pathway and temporo-ammonic pathway, respectively (41, 42). Along these lines, lesions of medial entorhinal cortex (MEC) layer 3 cause a reduction in spatial coherence of CA1 place cells (43), and impairments in excitatory neurons from MEC layer 3 have been reported in TLE (44). Multiple studies have shown a reduction in inhibitory synaptic input of MEC layer 2 neurons that innervate DG and CA3, resulting in increased synaptic input to these regions (17, 45, 46).

Past TLE research focused almost exclusively on place coding in a familiar environment or similar familiar environments (40), with little known about how the development and construction of new maps in novel environments would be impacted. We found that while control and KA mice formed distinct spatial representations between familiar and novel environments across hippocampal subregions, there was an impairment in the spatial stability of the newly formed place maps in CA3 of KA mice. Seminal research on remapping in the hippocampus has shown that distinct spatial maps are formed in novel environments but stabilized at different rates in the main hippocampal subregions of healthy, control animals (10, 47). Specifically, newly formed place maps from CA3 take longer to stabilize than CA1 when introduced to a novel environment – and our findings suggest this stabilization is exacerbated in epilepsy, which may point to augmentation of recurrence in CA3 (48). Novelty has been shown to drive DG granule cells and switch downstream CA3 networks into a state of forming new memories (i.e., spatial representations) rather than recalling previously formed maps (49). In TLE, this switch could be altered by the loss of inhibition from DG, resulting in a stronger drive to CA3 to form new maps and thus a destabilization across multiple exposures to the same novel environment.

CONCLUSIONS

In the epileptic brain, we found a decrease in the proportion of place cells in CA1 while exploring a familiar environment. Additionally, place fields of CA1 and CA3 cells were less coherent, while DG place maps were less stable. To further assess mechanisms of remapping and stability of newly formed place maps, we performed recordings while mice

explored a novel environment and found that all subregions constructed new, distinct maps within the first session of exposure to a novel environment, however new maps in CA3 were not stable in epileptic mice. Together, our findings highlight that focal TLE causes impairments in the spatial codes of place cells across hippocampal subfields CA1, CA3, and DG. These subregion-specific impairments demonstrate how TLE impacts critical memory circuits and provide a lens into how these impairments could disrupt memory flexibility and cognition.

ACKNOWLEDGEMENTS

NIH R01 1R01NS128222 (to L.A.E.), American Epilepsy Society Grant 835029 (to L.A.E.), American Epilepsy Society Grant 1462229 (to B.L.B.), and National Institute of Neurological Disorders and Stroke Grant T32 5T32NS045540 (to B.L.B.).

AUTHOR CONTRIBUTIONS

BLB: Conceptualization (equal); Methodology (equal); Investigation (lead); Data Curation (lead); Formal Analysis (lead); Software (equal); Visualization (lead); Funding Acquisition (supporting); Supervision (equal); Writing – Original Draft Preparation (equal); Writing – Review and Editing (equal). CD: Investigation (supporting). GT: Formal Analysis (supporting); Software (equal); Visualization (supporting). LAE: Conceptualization (equal); Methodology (equal); Formal Analysis (supporting); Software (equal); Visualization (supporting); Funding Acquisition (lead); Resources (lead); Supervision (equal); Writing – Original Draft Preparation (equal); Writing – Review and Editing (equal). All authors contributed to and approved the final manuscript.

CONFLICT OF INTEREST STATEMENT

None of the authors have any conflict of interest to disclose.

REFERENCES

1. Butler CR, Zeman AZ. Recent insights into the impairment of memory in epilepsy: transient epileptic amnesia, accelerated long-term forgetting and remote memory impairment. Brain. 2008;131(Pt 9):2243-63.
2. Cano-Lopez I, Hampel KG, Garces M, Villanueva V, Gonzalez-Bono E. Quality of life in drug-resistant epilepsy: relationships with negative affectivity, memory, somatic symptoms and social support. J Psychosom Res. 2018;114:31-7.
3. Khalife MR, Scott RC, Hernan AE. Mechanisms for Cognitive Impairment in Epilepsy: Moving Beyond Seizures. Front Neurol. 2022;13:878991.
4. Liu X, Muller RU, Huang LT, Kubie JL, Rotenberg A, Rivard B, et al. Seizure-induced changes in place cell physiology: relationship to spatial memory. J Neurosci. 2003;23(37):11505-15.
5. Lenck-Santini P-P, Holmes GL. Altered Phase Precession and Compression of Temporal Sequences by Place Cells in Epileptic Rats. The Journal of Neuroscience. 2008;28(19):5053-62.

6. Tyler AL, Mahoney JM, Richard GR, Holmes GL, Lenck-Santini PP, Scott RC. Functional network changes in hippocampal CA1 after status epilepticus predict spatial memory deficits in rats. J Neurosci. 2012;32(33):11365-76.
7. Barry JM, Sakkaki S, Barriere SJ, Patterson KP, Lenck-Santini PP, Scott RC, et al. Temporal Coordination of Hippocampal Neurons Reflects Cognitive Outcome Post-febrile Status Epilepticus. EBioMedicine. 2016;7:175-90.
8. Ewell LA, Fischer KB, Leibold C, Leutgeb S, Leutgeb JK. The impact of pathological high-frequency oscillations on hippocampal network activity in rats with chronic epilepsy. Elife. 2019;8.
9. Shuman T, Aharoni D, Cai DJ, Lee CR, Chavlis S, Page-Harley L, et al. Breakdown of spatial coding and interneuron synchronization in epileptic mice. Nat Neurosci. 2020;23(2):229-38.
10. Leutgeb S, Leutgeb JK, Treves A, Moser MB, Moser EI. Distinct ensemble codes in hippocampal areas CA3 and CA1. Science. 2004;305(5688):1295-8.
11. Lee I, Yoganarasimha D, Rao G, Knierim JJ. Comparison of population coherence of place cells in hippocampal subfields CA1 and CA3. Nature. 2004;430(6998):456-9.
12. Leutgeb JK, Leutgeb S, Moser MB, Moser EI. Pattern separation in the dentate gyrus and CA3 of the hippocampus. Science. 2007;315(5814):961-6.
13. Lee CH, Lee I. Impairment of Pattern Separation of Ambiguous Scenes by Single Units in the CA3 in the Absence of the Dentate Gyrus. J Neurosci. 2020;40(18):3576-90.
14. Tauck DL, Nadler JV. Evidence of functional mossy fiber sprouting in hippocampal formation of kainic acid-treated rats. J Neurosci. 1985;5(4):1016-22.
15. Buckmaster PS, Dudek FE. Network properties of the dentate gyrus in epileptic rats with hilar neuron loss and granule cell axon reorganization. J Neurophysiol. 1997;77(5):2685-96.
16. Buckmaster PS, Dudek FE. Neuron loss, granule cell axon reorganization, and functional changes in the dentate gyrus of epileptic kainate-treated rats. Journal of Comparative Neurology. 1997;385(3):385-404.
17. Kobayashi M, Buckmaster PS. Reduced inhibition of dentate granule cells in a model of temporal lobe epilepsy. J Neurosci. 2003;23(6):2440-52.
18. Santhakumar V, Aradi I, Soltesz I. Role of mossy fiber sprouting and mossy cell loss in hyperexcitability: a network model of the dentate gyrus incorporating cell types and axonal topography. J Neurophysiol. 2005;93(1):437-53.
19. Hofmann G, Balgooyen L, Mattis J, Deisseroth K, Buckmaster PS. Hilar somatostatin interneuron loss reduces dentate gyrus inhibition in a mouse model of temporal lobe epilepsy. Epilepsia. 2016;57(6):977-83.
20. Neunuebel JP, Knierim JJ. CA3 retrieves coherent representations from degraded input: direct evidence for CA3 pattern completion and dentate gyrus pattern separation. Neuron. 2014;81(2):416-27.
21. Cox BM, Cox CD, Gunn BG, Le AA, Inshishian VC, Gall CM, et al. Acquisition of temporal order requires an intact CA3 commissural/associational (C/A) feedback system in mice. Commun Biol. 2019;2:251.
22. Bedner P, Dupper A, Huttmann K, Muller J, Herde MK, Dublin P, et al. Astrocyte uncoupling as a cause of human temporal lobe epilepsy. Brain. 2015;138(Pt 5):1208-22.
23. Scharfman HE, Goodman JH, Sollas AL. Granule-like neurons at the hilar/CA3 border after status epilepticus and their synchrony with area CA3 pyramidal cells:

functional implications of seizure-induced neurogenesis. J Neurosci. 2000;20(16):6144-58.
24. Iyengar SS, LaFrancois JJ, Friedman D, Drew LJ, Denny CA, Burghardt NS, et al. Suppression of adult neurogenesis increases the acute effects of kainic acid. Exp Neurol. 2015;264:135-49.
25. Lisgaras CP, Scharfman HE. Robust chronic convulsive seizures, high frequency oscillations, and human seizure onset patterns in an intrahippocampal kainic acid model in mice. Neurobiol Dis. 2022;166:105637.
26. Voigts J, Newman JP, Wilson MA, Harnett MT. An easy-to-assemble, robust, and lightweight drive implant for chronic tetrode recordings in freely moving animals. J Neural Eng. 2020;17(2):026044.
27. Lopes G, Bonacchi N, Frazao J, Neto JP, Atallah BV, Soares S, et al. Bonsai: an event-based framework for processing and controlling data streams. Front Neuroinform. 2015;9:7.
28. Tarcsay G, Boublil BL, Ewell LA. Low-Cost Platform for Multianimal Chronic Local Field Potential Video Monitoring with Graphical User Interface (GUI) for Seizure Detection and Behavioral Scoring. eNeuro. 2022;9(5).
29. Yi JD, Pasdarnavab M, Kueck L, Tarcsay G, Ewell LA. Behavioral timing of interictal spikes, but not rate, correlates with impaired working memory performance. J Neurosci. 2025.
30. Pachitariu M, Steinmetz, N., Kadir, S., Carandini, M. & Harris, K. Fast and accurate spike sorting of high-channel count probes with KiloSort. . In: Lee DDea, editor. Proc 30th International Conference on Neural Information Processing Systems: Curran Associates; 2016. p. 4455–63
31. Mathis A, Mamidanna P, Cury KM, Abe T, Murthy VN, Mathis MW, et al. DeepLabCut: markerless pose estimation of user-defined body parts with deep learning. Nat Neurosci. 2018;21(9):1281-9.
32. Nath T, Mathis A, Chen AC, Patel A, Bethge M, Mathis MW. Using DeepLabCut for 3D markerless pose estimation across species and behaviors. Nat Protoc. 2019;14(7):2152-76.
33. Skaggs WE MB, Gothard KM, Markus EJ. . An information-theoretic approach to deciphering the hippocampal code1993. 1030–7 p.
34. Skaggs WE, McNaughton BL, Wilson MA, Barnes CA. Theta phase precession in hippocampal neuronal populations and the compression of temporal sequences. Hippocampus. 1996;6(2):149-72.
35. Muller RU, Kubie JL. The effects of changes in the environment on the spatial firing of hippocampal complex-spike cells. J Neurosci. 1987;7(7):1951-68.
36. Jones RT, Barth AM, Ormiston LD, Mody I. Evolution of temporal and spectral dynamics of pathologic high-frequency oscillations (pHFOs) during epileptogenesis. Epilepsia. 2015;56(12):1879-89.
37. Rusina E, Bernard C, Williamson A. The Kainic Acid Models of Temporal Lobe Epilepsy. eNeuro. 2021;8(2).
38. Bouilleret V, Loup F, Kiener T, Marescaux C, Fritschy JM. Early loss of interneurons and delayed subunit-specific changes in GABA(A)-receptor expression in a mouse model of mesial temporal lobe epilepsy. Hippocampus. 2000;10(3):305-24.

39. Zhang W, Yamawaki R, Wen X, Uhl J, Diaz J, Prince DA, et al. Surviving hilar somatostatin interneurons enlarge, sprout axons, and form new synapses with granule cells in a mouse model of temporal lobe epilepsy. J Neurosci. 2009;29(45):14247-56.
40. Ewell LA, Ramezani A, Suarez G, Piatti VC, Lam V, Mills TG, et al. Early impairment in dentate pattern separation in a rodent model of temporal lobe epilepsy. bioRxiv. 2025.
41. Witter MP, Groenewegen HJ, Lopes da Silva FH, Lohman AH. Functional organization of the extrinsic and intrinsic circuitry of the parahippocampal region. Prog Neurobiol. 1989;33(3):161-253.
42. Witter MP. Organization of the entorhinal-hippocampal system: a review of current anatomical data. Hippocampus. 1993;3 Spec No:33-44.
43. Brun VH, Leutgeb S, Wu HQ, Schwarcz R, Witter MP, Moser EI, et al. Impaired spatial representation in CA1 after lesion of direct input from entorhinal cortex. Neuron. 2008;57(2):290-302.
44. Feng Y, Diego KS, Dong Z, Christenson Wick Z, Page-Harley L, Page-Harley V, et al. Distinct changes to hippocampal and medial entorhinal circuits emerge across the progression of cognitive deficits in epilepsy. Cell Rep. 2025;44(2):115131.
45. Kumar SS, Buckmaster PS. Hyperexcitability, interneurons, and loss of GABAergic synapses in entorhinal cortex in a model of temporal lobe epilepsy. J Neurosci. 2006;26(17):4613-23.
46. Kumar SS, Jin X, Buckmaster PS, Huguenard JR. Recurrent circuits in layer II of medial entorhinal cortex in a model of temporal lobe epilepsy. J Neurosci. 2007;27(6):1239-46.
47. Leutgeb S, Leutgeb JK, Moser EI, Moser MB. Fast rate coding in hippocampal CA3 cell ensembles. Hippocampus. 2006;16(9):765-74.
48. Alme CB, Miao C, Jezek K, Treves A, Moser EI, Moser MB. Place cells in the hippocampus: eleven maps for eleven rooms. Proc Natl Acad Sci U S A. 2014;111(52):18428-35.
49. Gomez-Ocadiz R, Trippa M, Zhang CL, Posani L, Cocco S, Monasson R, et al. A synaptic signal for novelty processing in the hippocampus. Nat Commun. 2022;13(1):4122.

FIGURES AND TABLES

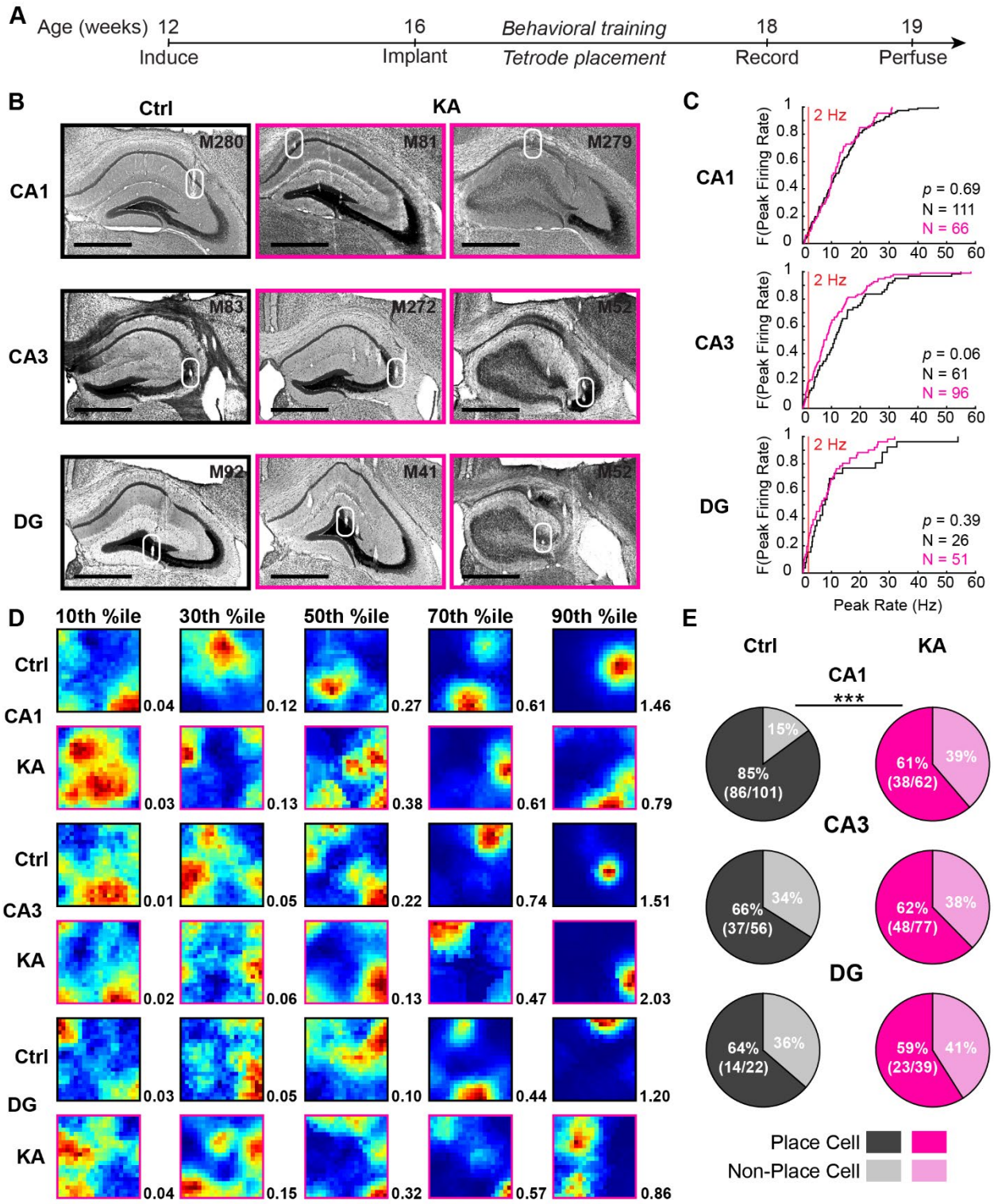

Figure 1. Experimental timeline and classification of place cells. ***A,*** Experimental timeline. At 12 weeks of age, mice were induced with a supra-hippocampal injection (AP: -2.00

mm from bregma, ML: +1.50 mm, DV: -0.8 mm, from dura) of kainic acid. Four weeks later, mice were implanted with an Open Ephys ShuttleDrive and hippocampal recordings were performed. ***B,*** Coronal sections through the hippocampus with tetrode tracks from control (black) and KA (pink) mice. The tetrode positions for recordings are indicated with a white circle for hippocampal CA1, CA3, and DG subregions. Scale bar, 870 µm. ***C,*** Cumulative distribution functions for peak firing rates in CA1, CA3, and DG of control and KA mice. There was no significant difference in peak firing rate between control and KA mice for CA1 ($z = 0.40$, $p = 0.69$), CA3 ($z = 1.89$, $p = 0.06$), and DG ($z = 0.86$, $p = 0.39$). Putative principal neurons were categorized as active if they had a peak firing rate ≥ 2 Hz. There was a significant difference in the percentage of active versus inactive principal neurons for CA3 ($\chi^2 = 3.87$, $p \leq 0.05$). There was no significant difference in the percentage of active versus inactive principal neurons for CA1 ($\chi^2 = 0.49$, $p = 0.48$) and DG ($\chi^2 = 0.69$, $p = 0.40$). ***D,*** Hippocampal single units recorded from CA1, CA3, and DG organized by spatial information for control and KA mice. Single units were detected using KiloSort and curated in Phy2. Putative principal neurons were distinguished from interneurons using a ≤ 10 Hz average firing rate cutoff. Spatial information was calculated for putative principal neurons and example rate maps are shown, organized from low to high spatial information. Spatial information (black) is indicated to the right of each example map. ***E,*** Proportion of place and non-place cells in CA1, CA3, and DG for control (dark/light grey) and KA (dark/light pink) mice. Place cells were distinguished from non-place cells using a shuffling procedure of spatial information. Single units were categorized as place cells if their spatial information was greater than the 95th percentile of the shuffled distribution and the peak rate was ≥ 2 Hz. Percentages of place and non-place cells are represented for each subregion in a pie chart, along with the number of place cells over the total number of cells recorded. There was a significant decrease in the proportion of place cells in CA1 of KA mice compared to controls ($\chi^2 = 12.01$, $p \leq 0.001$). There was no significant difference in the proportion of place cells between control and KA mice for CA3 ($\chi^2 = 0.20$, $p = 0.66$) and DG ($\chi^2 = 0.13$, $p = 0.72$). Wilcoxon rank sum test and Chi-squared test. Significance denoted with asterisks: ***p ≤ 0.001.

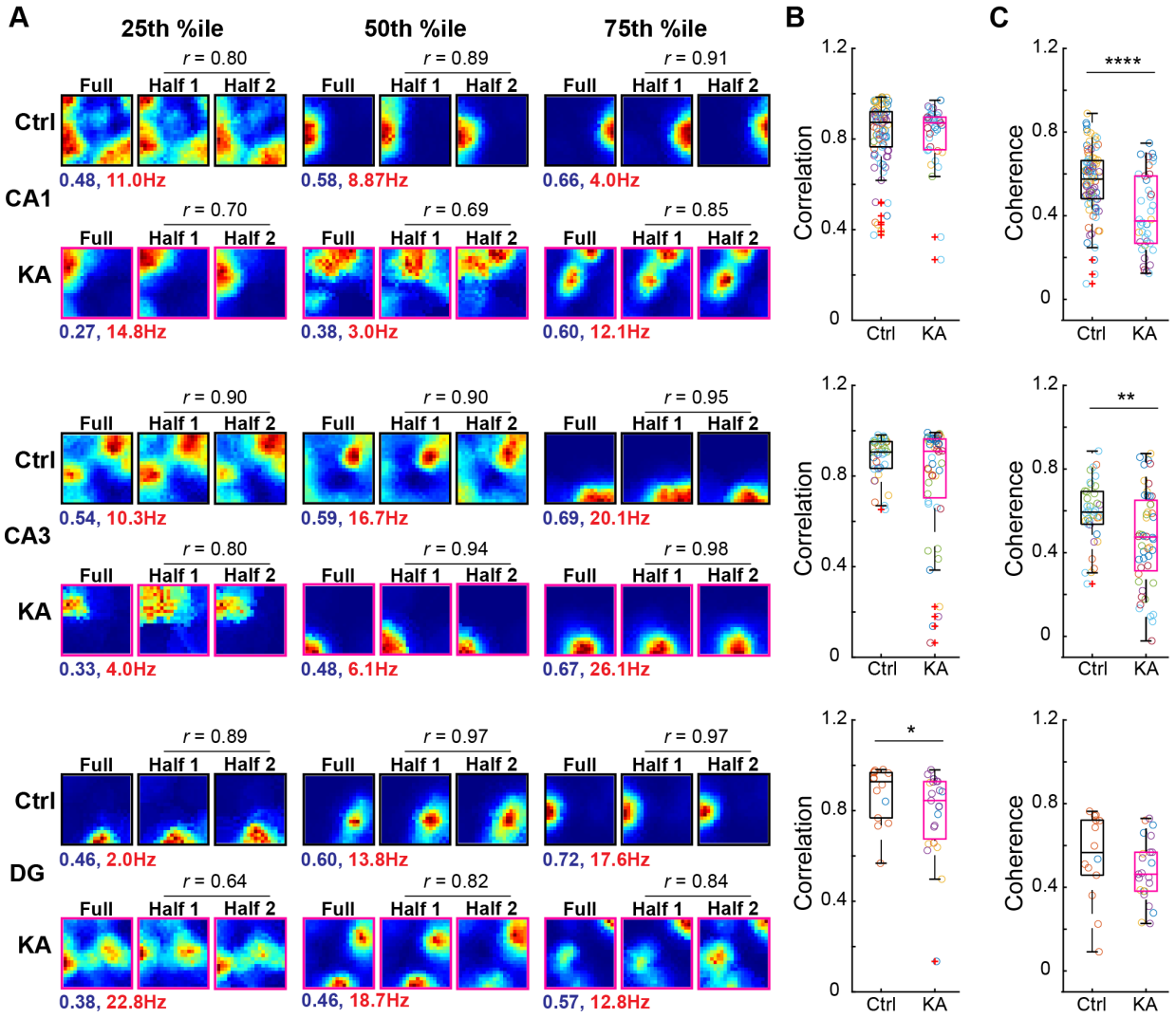

Figure 2. Spatial coherence decreased for hippocampal CA1 and CA3 in KA mice. ***A,*** Example rate maps of place cells from CA1, CA3, and DG for control (black) and KA (pink) mice. The maps shown were chosen based on the 25th, 50th, and 75th percentile for spatial coherence. For each example, the full map (left) and two half maps (right) are shown. The spatial coherence (blue) and peak firing rate (Hz, red) are indicated below each example map. The correlation between the first and second half for each map (black) is shown above each rate map example. ***B,*** Half map correlations of place cells from CA1, CA3, and DG for control (black) and KA (pink) mice. Box-and-whisker plots of correlations with the correlations for individual cells plotted as open circles. Median correlations are indicated with a solid line. There was no significant difference in the half map correlations between control and KA mice for CA1 (D = 0.18, p = 0.35) and CA3 (D = 0.21, p = 0.30). There was a significant decrease in the half map correlations KA mice for DG (D = 0.63, $p \leq 0.05$). ***C,*** Spatial coherence of place cells from CA1, CA3, and DG from control and KA mice. Box-and-whisker plots of spatial coherence with coherences for individual cells

plotted as open circles. Median coherences are indicated with a solid line. Spatial coherence significantly decreased in CA1 ($z = 3.95$, $p \leq 0.0001$) and CA3 ($z = 2.54$, $p \leq 0.01$) of KA mice compared to controls. There was no significant difference in spatial coherence between control and KA mice for DG ($z = 1.36$, $p = 0.17$). There was increased variance in spatial correlation ($F(36,47) = 0.13$, $p \leq 0.0001$) and spatial coherence ($F(36,47) = 0.43$, $p \leq 0.01$) in CA3 of KA mice. Two-sample Kolmogorov-Smirnov test, Wilcoxon rank sum test, and Two-sample F-test for equal variances, with Bonferroni's correction for multiple comparisons. Significance denoted with asterisks: *$p \leq 0.05$, **$p \leq 0.01$, ***$p \leq 0.001$, and ****$p \leq 0.0001$.

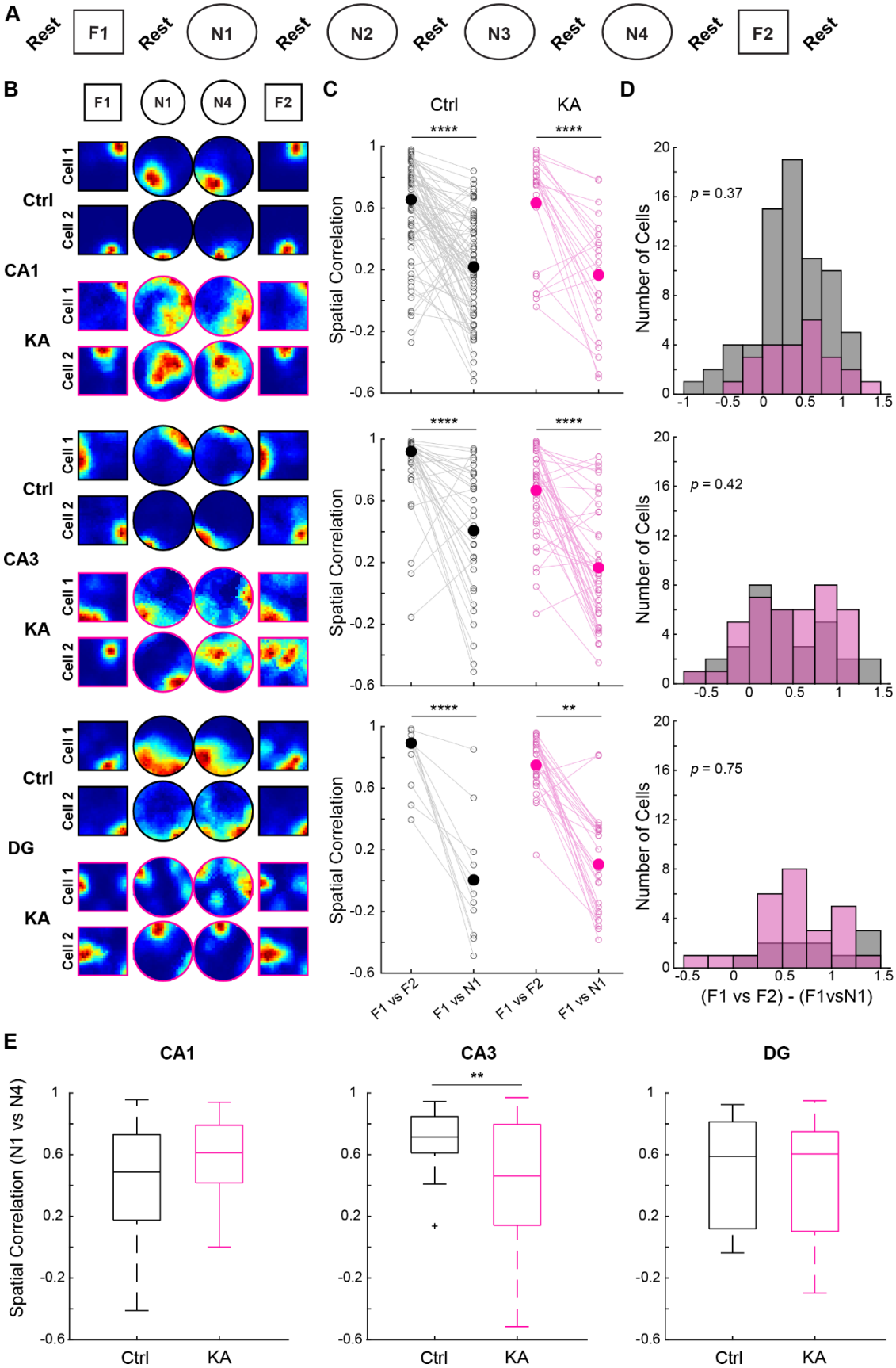
A
Rest
F1
Rest
N1
Rest
N2
Rest
N3
Rest
N4
Rest
F2
Rest
B
F1
N1
N4
F2
Ctrl
CA1
KA
CA3
DG
Cell 1
Cell 2
C
Ctrl
KA
Spatial Correlation
****
**
F1 vs F2
F1 vs N1
D
Number of Cells
p = 0.37
p = 0.42
p = 0.75
(F1 vs F2) - (F1vsN1)
E
CA1
CA3
DG
Spatial Correlation (N1 vs N4)
Ctrl
KA

Figure 3. Stability of place coding in a novel environment decreased for hippocampal CA3 of KA mice. ***A,*** Schematic of the novel room experimental paradigm. The experiment began with a 20-minute rest session before the first foraging session, followed by six 10-minute foraging sessions with 5 minutes of rest in between. The experiment concluded with a 20-minute rest session after the last foraging session. The foraging session sequence began with one session in the familiar arena (F1), followed by four sessions in the novel arena (N1-N4), and ended with one session back in the same familiar arena (F2). ***B,*** Example rate maps for individual place cells from hippocampal subregions CA1, CA3, and DG for control (black) and KA (pink) mice. ***C,*** Spatial correlations for comparisons between F1-F2 and F1-N1 for hippocampal CA1, CA3, and DG from control and KA mice. The median spatial correlation for each comparison is plotted as solid circles with spatial correlations for each individual cell plotted as paired, open circles. Spatial correlation significantly decreased between F1-F2 and F1-N1 for CA1 in control ($z = 5.47$, $p \leq 0.0001$) and KA ($z = 3.66$, $p \leq 0.001$) mice, as well as for CA3 in control ($z = 3.72$, $p \leq 0.001$) and KA ($z = 4.62$, $p \leq 0.0001$) mice, and DG in control (z = n/a, $p \leq 0.001$) and KA ($z = 4.33$, $p \leq 0.0001$) mice. ***D,*** Distribution of place cell spatial correlations for the difference between F1-F2 and F1-N1. There was no significant difference between distributions of control and KA mice in CA1 ($z = -0.90$, $p = 0.37$), CA3 ($z = -0.80$, $p = 0.42$), or DG ($z = 0.45$, $p = 0.75$). ***E,*** Spatial correlations of place cells from comparisons of N1-N4 for hippocampal CA1, CA3, and DG from control and KA mice. Box-and-whisker plots are shown for each hippocampal subregion for control and KA mice. The median spatial correlations are indicated as a solid line. There was a significant decrease in N1-N4 spatial correlation for CA3 for KA compared to control mice ($z = 2.46$, $p \leq 0.01$), but no significant difference between control and KA mice for CA1 ($z = -1.39$, $p = 0.16$) or DG ($z = 0$, $p = 1$). Wilcoxon signed rank test and Wilcoxon rank sum test, with Bonferroni's correction for multiple comparisons. Significance is denoted with asterisks: *$p \leq 0.05$, **$p \leq 0.01$, ***$p \leq 0.001$ and ****$p \leq 0.0001$.

Table 1. Interictal spike (IS) rate with spike detection parameters for each KA mouse, during rest and during behavior.

Mouse ID	IS rate during rest (spikes/s)	IS rate during behavior (spikes/s)	Threshold (μV)	Low pass-band (Hz)	High pass-band (Hz)
M41	0.4962	0.0066	400	1	400
M42	0.3683	0.1925	400	1	400
M52	0.2448	0.1781	400	1	400
M81	0.0058	0.0017	1000	1	400
M90	0.0039	0.0013	400	1	400
M227	0.2911	0.1782	500	1	400
M272	0.1083	0.0282	800	1	400
M279	0.9137	0.5151	300	1	400
M321	0.0494	0	800	1	400
M322	0.0058	0.0017	900	1	400

Table 2. Peak rate firing distributions for active and inactive principal cells.

Hippocampal Subregion	Experimental Group	Active Principal Cells	Inactive Principal Cells
CA1	Control	12.83; 7.39-18.35 (N = 101)	1.39; 0.67-1.75 (N = 10)
	KA	11.43; 7.72-18.34 (N = 62)	0.86; 0.69-0.94 (N = 4)
CA3	Control	11.84; 6.40-20.39 (N = 56)	0.54; 0.06-0.76 (N = 5)
	KA	9.48; 6.31-15.40 (N = 77)	1.12; 0.81-1.57 (N = 19)
DG	Control	8.62; 4.97-25.27 (N = 22)	1.11; 0.59-1.45 (N = 4)
	KA	9.13; 4.71-15.69 (N = 39)	0.83; 0.36-1.45 (N = 12)

For each hippocampal subregion and experimental group, the median and interquartile ranges (median; IQR) of peak firing rate distributions for active and inactive principal cells are listed.

Table 3. Additional properties of place cells for hippocampal CA1, CA3, and DG.

Region	Group	Peak Rate (Hz)	Sparsity	Selectivity	Statistics
CA1	Control (N = 86)	10.93; 6.64-17.57	0.54; 0.31-0.75	4.98; 3.11-8.14	$z_{PeakRate}$ = 0.09, p = 0.92 $z_{Sparsity}$ = 0.76, p = 0.45 $z_{Selectivity}$ = -0.73, p = 0.47
	KA (N = 38)	11.43; 6.16-19.49	0.46; 0.40-0.55	5.51; 4.20-7.90	
CA3	Control (N = 37)	12.52; 6.90-21.33	0.42; 0.22-0.74	6.04; 3.42-10.91	$z_{PeakRate}$ = 1.01, p = 0.31 $z_{Sparsity}$ = 0.99, p = 0.32 $z_{Selectivity}$ = -0.91, p = 0.36
	KA (N = 48)	10.09; 5.13-20.29	0.38; 0.12-0.54	8.27; 4.71-20.59	
DG	Control (N = 14)	9.13; 4.97-22.96	0.43; 0.19-0.68	7.49; 4.27-18.02	$z_{PeakRate}$ = -0.05, p = 0.96 $z_{Sparsity}$ = -0.77, p = 0.44 $z_{Selectivity}$ = 1.11, p = 0.27
	KA (N = 23)	11.21; 6.29-19.57	0.50; 0.38-0.64	5.50; 3.72-8.64	

For each hippocampal region and experimental group, the median and interquartile ranges (median; IQR) for each property of place cells are listed. Results of Wilcoxon rank sum test are reported for peak rate, sparsity, and selectivity, respectively. There were no significant differences between control and KA mice for these place cell properties.

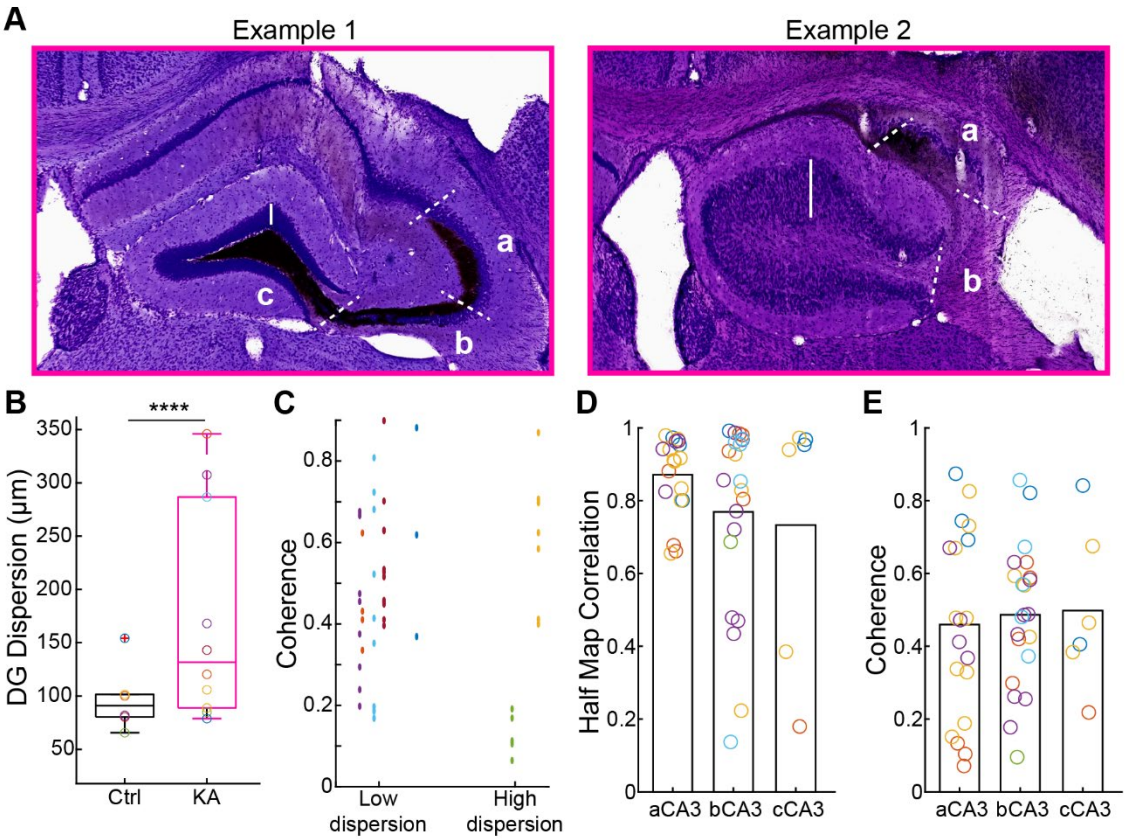

Figure S1. Histopathology and properties of place cells in the supra-hippocampal kainic acid mouse model of focal temporal lobe epilepsy. ***A,*** Histological examples of hippocampal sections from KA mice. Sections were stained with cresyl violet to visualize cell layers of the hippocampus (purple) and TIMM-stained to visualize mossy fibers (brown). The subareas of hippocampal CA3 (a, b, and c) are indicated with a dashed line and labeled accordingly. CA3 cells were included in one of the three subareas based on the histological reconstruction of the final recording location of CA3 tetrodes. The thickness of the dentate gyrus (DG) is indicated by a white bar in each example image. ***B,*** DG dispersion comparison between control and KA mice. DG dispersion was determined by an investigator that manually measured the thickness of the upper blade of the DG for three consecutive sections of dorsal hippocampus, ipsilateral to the KA injection, for each mouse. The thickness for the three sections were averaged to obtain a measure of DG dispersion for each mouse. There was a significant increase in DG dispersion in KA mice compared to control mice ($z = -5.27$, $p \leq 0.0001$). ***C,*** Spatial coherence of CA3 as a function of DG dispersion for KA mice. DG dispersion scores were divided into low (< 200 µm) and high (≤ 200 µm) dispersion groups and plotted against the spatial coherence of hippocampal CA3. There was no significant difference in spatial coherence between low and high dispersion groups ($z = 0.34$, $p = 0.73$). ***D,*** Half map correlation for subareas of hippocampal CA3. Half map correlations for CA3 place cells plotted for each subarea of CA3, with individual cells plotted as open circles. There was

no significant difference in half map correlation between the subareas of CA3 ($F = 1.40$, $p = 0.26$). ***E,*** Spatial coherence for subareas of hippocampal CA3. Spatial coherence for CA3 place cells plotted for each subarea of CA3, with individual cells plotted as open circles. There was no significant difference in spatial coherence between the subareas of CA3 ($F = 1.05$, $p = 0.90$). Wilcoxon rank sum test and one-way ANOVA. Significance denoted with asterisks: ****$p \leq 0.0001$.